International Journal of Naval Architecture and Ocean Engineering 12 (2020) 468–478

Contents lists available at ScienceDirect

International Journal of Naval Architecture and Ocean Engineering

journal homepage: http://www.journals.elsevier.com/international-journal-of-naval-architecture-and-ocean-engineering/

Hydrodynamic performance of a vertical slotted breakwater

Arun George, Il Hyoung Cho*

Department of Ocean System Engineering, Jeju National University, Jeju, 690-756, Republic of Korea

ARTICLE INFO

Article history:
Received 2 April 2019
Received in revised form
2 October 2019
Accepted 3 December 2019
Available online 10 December 2019

Keywords:
Slotted breakwater
Energy dissipation
Nonlinear porous boundary condition
Eigenfunction expansion method
K-epsilon turbulent model

ABSTRACT

The wave interaction problem with a vertical slotted breakwater, consisting of impermeable upper, lower parts and a permeable middle part, has been studied theoretically. An analytical model was presented for the estimation of reflection and transmission of monochromatic waves by a slotted breakwater. The far-field solution of the wave scattering involving nonlinear porous boundary condition was obtained using eigenfunction expansion method. The empirical formula for drag coefficient in the near-field, representing energy dissipation across the slotted barrier, was determined by curve fitting of the numerical solutions of 2-D channel flow using CFD code StarCCM+. The theoretical model was validated with laboratory experiments for various configurations of a slotted barrier. It showed that the developed analytical model can correctly predict the energy dissipation caused by turbulent eddies due to sudden contraction and expansion of a slotted barrier. The present paper provides a synergetic approach of the analytical and numerical modelling with minimum CPU time, for better estimation of the hydrodynamic performance of slotted breakwater.

1. Introduction

The traditional breakwater, such as rubble mound breakwater, has many disadvantages in terms of environmental and economic aspects. For the last several decades, many researchers have been focusing on overcoming these demerits and consequently, sea-exchanging porous breakwaters have emerged. These kinds of breakwaters reduce the potential erosion on the down-drift side and allow a continuous exchange of the water masses. It is effective, especially at the places where the soil has a low load bearing capacity. In addition, the construction period is short and the cost can be reduced. Despite the growing concern of such structures, relatively little comprehensive design information is available on their hydrodynamic characteristics.

Many studies have been accomplished in the past by many researchers to propose a new type of permeable breakwaters and to evaluate its hydrodynamic performance. The analytical, numerical, and experimental studies for wave scattering by a vertical permeable breakwater have been conducted. Hayashi et al., (1966) studied the hydraulic properties of a row of closely spaced circular piles as a breakwater, theoretically and experimentally. Their theoretical model can predict the wave transmission and moment distribution for the circular pile breakwater. Sollit and Cross, (1972) derived a theory to predict the wave reflection and transmission of a permeable slotted breakwater composed of slots and slats. Grüne and Kohlhase, (1974) represented the transmission coefficient for the vertical slotted barrier as a function of porosity, local geometry of slots and slats and heading angle of incident waves through the series of experiments. Mei et al., (1974) suggested the porous nonlinear boundary condition, which represents the energy loss due to surface elevation drop proportional to the square of the local velocity, and showed the effects of higher harmonic components generated by a porous barrier. Kriebel, (1993) carried out a theoretical analysis of wave interaction with a vertical slotted breakwater based on the application of the continuity, momentum, and energy equations to flow through the slots. He suggested the simple expressions for the wave transmission coefficient and wave forces on the wall. Kakuno and Liu, (1993) studied the wave scattering by an array of vertical cylinders theoretically and experimentally. In their study, energy loss due to the flow separation near the cylinders was modeled by adopting a linearized form of the quadratic resistance law. Suh and Park, (1995) developed the analytical model that predicts the reflection from perforated-wall caisson breakwater using the Galerkin-eigenfunction method. Isaacson et al., (1998) outlined a numerical calculation of wave interactions with a partially submerged vertical slotted barrier. The numerical model

* Corresponding author.
E-mail addresses: arunmvgeorge@gmail.com (A. George), cho0904@jejunu.ac.kr (I.H. Cho).
Peer review under responsibility of Society of Naval Architects of Korea.

https://doi.org/10.1016/j.ijnaoe.2019.12.001

was solved by the eigenfunction expansion method utilizing Darcy's law as a boundary condition at the porous barrier. Darcy's law demonstrated that the velocity at the porous plate with relatively fine pores is linearly proportional to the pressure drop. They also conducted laboratory tests to validate the proposed theoretical model. Suh et al., (2006) presented the numerical results for a single vertical slotted breakwater with impermeable upper and lower parts and permeable part in the middle with different heights and validated theoretical solution by comparison of experimental results. Huang, (2007) investigated the wave interaction with one or two rows of closely spaced slotted barriers, theoretically and experimentally. An empirical expression was proposed for the friction coefficient which models the head loss due to closely spaced slotted barriers. Cho and Kim, (2008) developed an analytical model using Darcy's law based on an eigenfunction expansion method for the design of an effective wave-absorption system. The developed theory was verified by both small-scale and full-scale experiments. Suh et al., (2011) estimated the friction coefficient of a perforated wall on the basis of the best fit between measured and predicted values of reflection and transmission coefficients. Ahmed, (2011) developed an analytical model based on an eigenfunction expansion method for regular wave interactions with single and double vertical slotted barriers. They validated the analytical model by comparing its results with those of previous studies and their own experimental results. Crowley and Porter, (2012) and Molin and Remy, (2013) proposed a quasi-linear model for wave energy dissipation through a thin vertical porous barrier, where both the inertial and quadratic drag forces were included. The quadratic drag term was linearized by equivalent linearization. Their analytical models were then applied to a range of wave scattering and sloshing problems. Somervell et al., (2017) studied hydrodynamic characteristics of a vertical cellular breakwater with double barriers and different porosities of the upper and lower parts. The eigenfunction expansion method was used to develop a theoretical model to study the hydrodynamic performance of the cellular breakwater.

In the present paper, a theoretical model was formulated for investigating the wave reflection and transmission by a vertical slotted breakwater, by adopting the methodology similar to Crowley and Porter, (2012) and Molin and Remy, (2013). In particular, the empirical formula for the drag coefficient, representing the energy dissipation across the slotted barrier, was derived through curve fitting with numerical results. The numerical solutions in near-field were obtained by solving the 2-D channel flow past symmetric slats with a centered slot with the help of StarCCM+. Far-field solutions involving a nonlinear porous boundary condition were solved by an iterative scheme based on eigenfunction expansion method. Calculation model of a slotted barrier was composed of three parts; the impermeable upper and lower part, and the permeable middle part in-between them. Through verifying the reliable correlation between the predicted values and experimental data conducted by Ahmed, (2011), the present prediction tool was proved to correctly predict the energy dissipation due to turbulent eddies generated near a slotted barrier. It is found that the porosity of a slotted barrier plays an important role in energy dissipation, but the effect of Reynold's number and thickness of barrier is negligible.

2. Mathematical formulation

The small-amplitude waves of a single angular frequency (ω) and amplitude (A) propagate normally to a vertical slotted breakwater locating at $x = 0$ in constant water depth h. d_1 is the height of the upper impermeable part; $d_2 - d_1$ is the height of the middle permeable part. The permeable part is composed of the array of rectangular slats of height w, thickness b and slots of gap c. The resulting fluid motion is assumed to be two-dimensional. The fluid is incompressible and inviscid, and the flow is assumed to be irrotational. Thus, we can introduce the velocity potential Φ The eigenfunctions (x, z, t) satisfying

$$\nabla^2 \Phi = 0. \tag{1}$$

$$g\frac{\partial \Phi}{\partial z} + \frac{\partial^2 \Phi}{\partial t^2} = 0, \ \text{on} \ z = 0. \tag{2}$$

$$\frac{\partial \Phi}{\partial z} = 0, \ \text{on} \ z = -h. \tag{3}$$

where g is gravitational acceleration.

We need additional boundary conditions relating properties of the flow on one side of the permeable barrier to the other. Crowley and Porter, (2012) and Molin and Remy, (2013) allow us to formulate following boundary conditions on the slotted barrier. The first boundary condition is to be the continuity of horizontal velocity across the barrier,

$$\left[\frac{\partial \Phi}{\partial x}\right]_{x=0^-}^{x=0^+} = 0, \ \text{on} \ x = 0, \ -h \le z \le 0. \tag{4}$$

The second boundary condition can be written in the following equation depending on whether it belongs to permeable or impermeable boundary.

$$\begin{aligned} &\frac{\partial \Phi}{\partial x} = 0, \ \text{on} \ x = 0, -d_1 \le z \le 0, -h \le z \le -d_2, \\ &\left[\frac{\partial \Phi}{\partial t}\right]_{x=0^-}^{x=0^+} = \frac{1}{2} C_D U(z,t)|U(z,t)| + 2C\frac{\partial U}{\partial t}(z,t), \ \text{on} \ x = 0, -d_2 \le z \le -d_1. \end{aligned} \tag{5}$$

where $U(z,t) = \frac{\partial \Phi}{\partial x}(0,z,t)$ is the horizontal fluid velocity at the barrier and C_D and $2C$ represent the drag coefficient relating to energy dissipation and the blockage (inertial) coefficient accounting for the added inertia felt by the fluid as it accelerates through the sudden constrictions in a slotted barrier. These coefficients can be determined empirically with the help of the idealized analytical and numerical solution.

Assuming harmonic motion of frequency ω, the velocity potential can be written as

$$\Phi(x,z,t) = \mathrm{Re}\left\{ -\frac{igA}{\omega}\phi(x,z)e^{-i\omega t} \right\}. \tag{6}$$

The complex velocity potential ϕ satisfies Laplace equation

$$\nabla^2\phi = 0, \quad \text{in the fluid.} \tag{7}$$

with the following boundary conditions

$$\frac{\partial\phi}{\partial z} + \frac{\omega^2}{g}\phi = 0, \ \text{ on } \ z = 0. \tag{8}$$

$$\frac{\partial\phi}{\partial z} = 0, \ \text{ on } \ z = -h. \tag{9}$$

$$\lim_{|x|\to\infty}\left(\frac{\partial\phi}{\partial|x|} - ik\phi\right) = 0. \tag{10}$$

In order to add the viscosity effect in the linear potential theory, the entire fluid region is divided into the far-field and near-field region. The solution in each region is governed by different length scales. We approximate the governing equation and boundary conditions according to the local scales and seek solutions valid in these separate regions.

2.1. FAR-FIELD solution

Let us define the far-field to be the region which is at a distance $O(k^{-1})$ away from the slotted barrier. At a far distance from the slotted barrier, the local shape of the slotted barrier is invisible, and the incident, reflected, and transmitted waves by a slotted barrier are only seen to the far-field observer. We can write the velocity potential in $x < 0$ and $x > 0$ satisfying Eqs. (7)–(10) as

$$\begin{aligned}\phi_1(x,z) &= \sum\nolimits_{n=0}^{\infty}\left(e^{-k_n x}\delta_{n0} + A_n e^{k_n x}\right)f_n(z), \quad x \le 0,\\ \phi_2(x,z) &= \sum_{n=0}^{\infty} B_n e^{-k_n x} f_n(z), \quad x > 0.\end{aligned} \tag{11}$$

The eigenfunctions $f_n(z)$ in Eq. (11) are defined as

$$f_n(z) = \frac{\cos k_n(z+h)}{\cos k_n h}, \quad n = 0, 1, 2, \ldots. \tag{12}$$

where k_n $(n \ge 1)$ are the real positive roots of $k_n \tan k_n h = -\omega^2/g$ while $k_0 = -ik$ where k is the real positive root of $k \tanh kh = \omega^2/g$.

The eigenfunctions $f_n(z)$ are complete on the interval [-*h*, *0*], therefore satisfy the following orthogonal relation

$$\int_{-h}^{0} f_m(z) f_n(z)\,dz = N_n\delta_{mn}, \tag{13}$$

where $N_n = \frac{1}{\cos^2 k_n h}\left(\frac{h}{2} + \frac{\sin 2k_n h}{4k_n}\right)$, δ_{mn} in Eqs. (11) and (13) is the Kronecker delta function defined by $\delta_{mn} = 1$ if $m = n$, and $\delta_{mn} = 0$ if $m \ne n$.

The horizontal fluid velocity $u(z)$ at $x = 0$, satisfying the continuity equation, can be expressed by the series of eigenfunctions $f_n(z)$

$$\frac{\partial\phi_1}{\partial x}(0,z) = \frac{\partial\phi_2}{\partial x}(0,z) = u(z) = \sum_{n=0}^{\infty} k_n u_n f_n(z). \tag{14}$$

If substituting Eq. (11) into the equation Eq. (14), the unknowns A_n, B_n can be expressed by u_n as follows:

$$\begin{aligned}A_n &= u_n + \delta_{n0},\\ B_n &= -u_n.\end{aligned} \tag{15}$$

If substituting Eq. (15) into Eq. (11), the velocity potential can be rewritten as

$$\begin{aligned}\phi_1(x,z) &= \sum_{n=0}^{\infty}\left[\left(e^{-k_n x} + e^{k_n x}\right)\delta_{n0} + u_n e^{k_n x}\right]f_n(z), \quad x \le 0,\\ \phi_2(x,z) &= -\sum_{n=0}^{\infty} u_n e^{-k_n x} f_n(z), \quad x > 0.\end{aligned} \tag{16}$$

The unknown coefficients $u_n, (n = 0, 1, \ldots)$ can be determined by using the remaining boundary condition Eq. (5). The quadratic velocity dependence in Eq. (5) implies that incident wave excitation with a single frequency ω introduces multi-frequency wave responses due to the nonlinear boundary condition. Thus, expanding Φ in a Fourier time-series in multiples of ω and retaining just the fundamental frequency response (the Fourier coefficient of first term is $8/3\pi$ while the next term at frequency 3ω is much smaller than ω and justifies this assumption) transforms Eq. (5) b into following equivalent linear boundary condition.

$$u(z) = \begin{cases} 0, & \text{on} \quad -d_1 \le z \le 0,\\ -i\sigma(z)[\phi(0^+,z) - \phi(0^-,z)], & \text{on} \quad -d_2 \le z \le -d_1,\\ 0, & \text{on} \quad -h \le z \le -d_2.\end{cases} \tag{17}$$

where $\sigma(z) = \frac{1}{\frac{\beta(z)}{\omega} - 2iC}$ with $\beta(z) = \frac{4C_D g A}{3\pi\omega}|u(z)|$, $|\ |$ denotes the modulus of the complex number.

If substituting the expression of velocity potential in Eq. (16) into Eq. (17), mixed boundary conditions along z-axis can be obtained as follows:

$$\sum_{n=0}^{\infty} k_n u_n f_n(z) = \begin{cases} 0, & \text{on} \quad -d_1 \le z \le 0,\\ 2i\bar{\sigma}\sum_{n=0}^{\infty}(u_n + \delta_{n0})f_n(z), & \text{on} \quad -d_2 \le z \le -d_1,\\ 0, & \text{on} \quad -h \le z \le -d_2.\end{cases} \tag{18}$$

where $\bar{\sigma} = \frac{1}{d_2 - d_1}\int_{-d_2}^{-d_1}\sigma(z)dz$ is defined by its averages over the porous vertical barrier.

Multiplying both sides of Eq. (18) by $\{f_m(z) : m = 0, 1, 2, \ldots\}$ and integrating with respect to from -*h* to 0, we obtain the nonlinear algebraic equations taking the first N terms in the infinite series.

$$\begin{aligned}&\sum_{n=0}^{N}\{k_n N_n\delta_{mn} - 2i\bar{\sigma}S_{mn}(-d_2, -d_1)\}u_n\\ &\quad = 2i\bar{\sigma}S_{m0}(-d_2, -d_1), \quad m = 0, 1, 2, \ldots, N\end{aligned} \tag{19}$$

where $\bar{\sigma} = \dfrac{1}{\frac{4C_D g A}{3\pi\omega^2}\left|\sum_{n=0}^{N}\frac{u_n}{d_2 - d_1}\int_{-d_2}^{-d_1} f_n(z)dz\right| - 2iC}$,

$$S_{mn}(p,q) = \int_p^q f_m(z) f_n(z)dz = \frac{1}{2\cos k_m h\cos k_n h}\left[\frac{\sin(k_m + k_n)(z+h)}{k_m + k_n} + \frac{\sin(k_m - k_n)(z+h)}{k_m - k_n}\right]_p^q.$$

We solved the nonlinear algebraic Eq. (19) by implementing the Newton–Raphson iterative scheme.

$$\sum_{n=0}^{N}\left\{k_n N_n \delta_{mn} - 2i\overline{\sigma}^{(l-3/2)} S_{mn}(-d_2,-d_1)\right\} u_n^{(l)} = 2i\overline{\sigma}^{(l-3/2)} S_{m0}(-d_2,-d_1), \quad m = 0,1,2,...,N \tag{20}$$

The superscript (l) in Eq. (20) means the present iteration step. $\overline{\sigma}^{(l-3/2)}$ at iteration step $(l-3/2)$ means to be calculated from the averaged values $(u_n^{(l-2)} + u_n^{(l-1)})/2$ between the previous two iteration steps $(l-2)$ and $(l-1)$. In this way, relaxation is introduced in the iterative scheme and convergence is faster. Convergence to give a desired accuracy $\left|u_n^{(l+1)} - u_n^{(l)}\right| \le 10^{-6}$ is reached within 10–20 iterations with $u_n^{(1)}, (n = 0,1,2,..,N)$ initially taken equal to 0 under the assumption of no obstruction.

Finally, the reflection R_f and transmission coefficients T_r of the vertical slotted breakwater, can be determined from:

$$R_f = |1 + u_0|, \quad T_r = |-u_0|. \tag{21}$$

The energy loss coefficient ε_L across the slotted barrier is defined by

$$\varepsilon_L = 1 - R_f^2 - T_r^2. \tag{22}$$

The horizontal wave forces ($F = \mathrm{Re}\{f\, e^{-i\omega t}\}$) on the vertical slotted barrier can be calculated by integrating the dynamic pressure along the barrier.

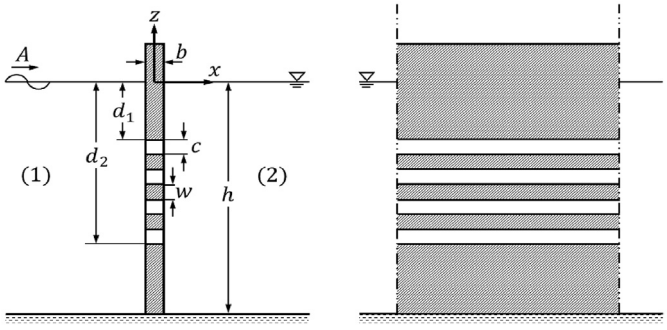

Fig. 1. Definition sketch of a vertical slotted breakwater.

$$f = \rho g A \int_{-h}^{0} [\phi_1(0,z) - \phi_2(0,z)]dz = 2\rho g A \sum_{n=0}^{N} (\delta_{n0} + u_n) \frac{\tan k_n h}{k_n}. \tag{23}$$

2.2. NEAR-FIELD solution

Near the slotted barrier, the length scale $O(c)$ is the opening gap of the slot; hence a near-field defined as the neighborhood of the slot (see Fig. 1). In the near-field, the governing equation is 2-D Laplace equation and the no-flux condition must be satisfied on the solid walls. The radiation condition is no longer relevant and has to be discarded. Therefore the near-field problem becomes that of the 2-D channel flow past symmetric slats (Fig. 2). Flagg and Newman, (1971) obtained the blockage coefficient for steady 2-D channel flow past a rectangular cylinder by means of matched asymptotic expansion method as follows:

$$2C = b\left(\frac{1}{P} - 1\right) + \frac{2(w+c)}{\pi}\left[1 - \log(4P) + \frac{1}{3}P^2 + \frac{281}{180}P^4\right] + O\left(P^6\right), \tag{24}$$

where the center-to-center spacing between adjacent slats is $w + c$. The porosity is defined by $P = c/(w+c)$.

In the near-field, we can also obtain the empirical formula of drag coefficient C_D from the curve fitting with the StarCCM + numerical results. The porosity, Reynolds number, and thickness of slotted breakwater play an important role on the drag coefficient C_D. Therefore numerical calculation was performed for five different porosities ($P = 0.079, 0.1264, 0.2272, 0.3269, 0.4265$),

Table 2
C_D versus upstream lengths. ($\mathrm{Re} = 1.5 \times 10^3$)

P	10w	15w	20w
0.0790	248.45	242.41	247.55
0.1264	81.74	81.06	80.61
0.2272	21.33	21.32	21.42
0.3269	8.52	8.46	8.48
0.4265	4.01	3.95	3.93

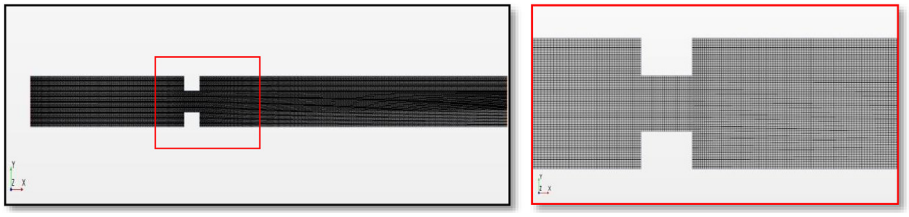

Fig. 2. Mesh generated over the fluid domain ($P = 0.4265$).

Table 1
Mesh convergence test for C_D.

Porosity (P)	Coarse (3×10^3 cells)	Normal (11×10^3 cells)	Fine (27×10^3 cells)	Very Fine (48×10^3 cells)
0.079	286.359	249.85	248.448	248.657
0.1264	95.178	87.971	81.74	81.24
0.2272	23.76	21.48	21.33	21.24
0.3269	9.788	8.665	8.521	8.475
0.4265	4.7686	4.085	4.0108	4.025

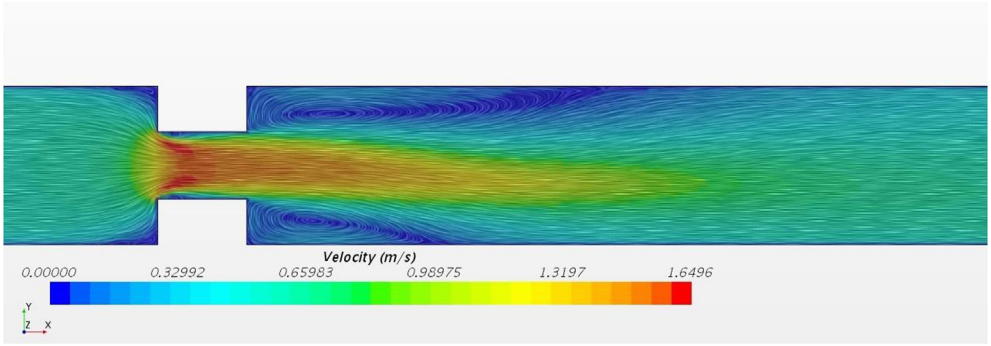

Fig. 3. Velocity pattern around near field of slotted barrier from StarCCM+ ($P = 0.4265,\ w = b = 2.5cm,\ \mathrm{Re} = 1.5 \times 10^4$).

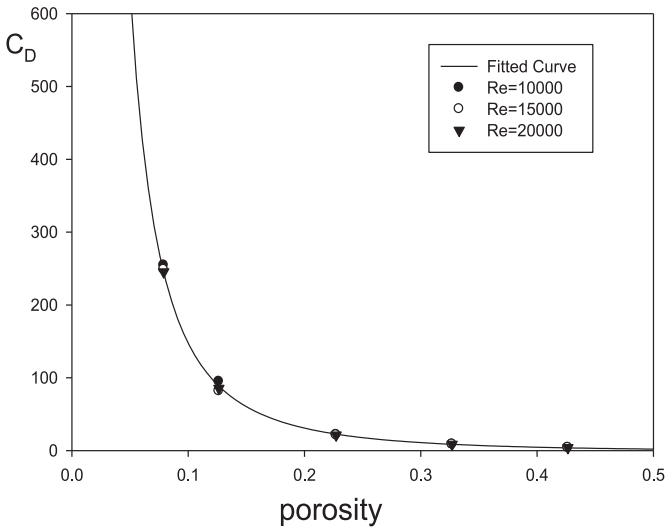

Fig. 4. Variation of C_D with Reynolds number.

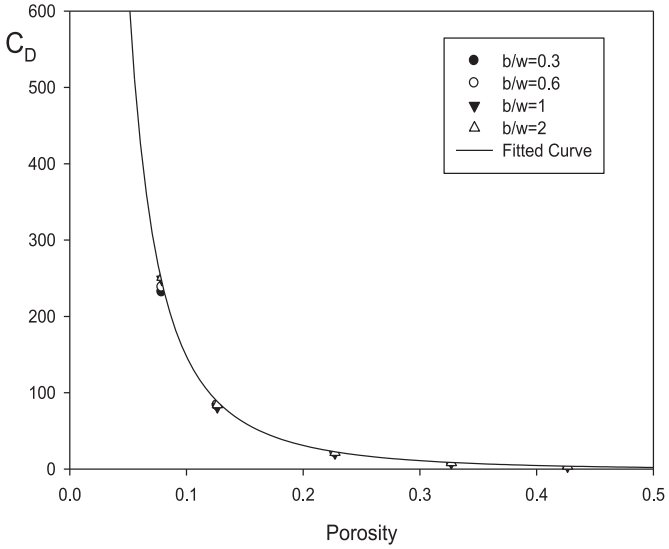

Fig. 5. Drag coefficients as a function of porosity and thickness ratio ($\mathrm{Re} = 1.5\times 10^3$).

three different upstream velocities, and four different thickness ratios (b/w) with fixed slat height ($w = 2.5$ cm). The upstream velocities (0.356,0.534,0.712 m/s) are set at the inlet boundary based on Re = 10,000,15000,20000. The outlet boundary is defined as a pressure outlet. All other boundaries are defined as rigid wall boundaries. Fig. 2 shows the discretized fluid domain with fine mesh for $P = 0.4265$.

For numerical calculation, the directed mesh tool in StarCCM+, which provides a high degree of control and accuracy, was used to discretize the fluid domain. A Flow-aligned mesh is created, and finer mesh size is generated near the slot and slat to capture the flow separation and turbulence eddies. The grading in mesh size along the upstream and downstream directions is accomplished by the hyperbolic stretching option.

Segregated steady solver and second-order upwind scheme were used for the numerical simulation. To incorporate the turbulence, the standard two layer $k-\varepsilon$ model was used. This model is the most widely used and pertinent model for confined turbulence flows. The transport equations for the turbulent kinetic energy k and turbulent dissipation rate ε were solve to determine the turbulent eddy viscosity μ_t.

The all-y + wall treatment was used here, which is a hybrid treatment that emulates the low-y + wall treatment for fine meshes, and the high-y + wall treatment for coarse meshes. This two-layer model solves for k but prescribes ε algebraically with distance from the wall in the viscosity dominated near-wall flow regions. The dissipation rate near the wall is simply prescribed as $\varepsilon = \frac{k^{3/2}}{l_\varepsilon}$, where l_ε is a length scale function depending upon the model variant. The turbulent viscosity $\mu_t|_{k-\varepsilon}$ from the $k-\varepsilon$ model is then blended with the two-layer value, as follows:

$$\mu_t = \lambda \mu_t|_{k-\varepsilon} + (1-\lambda)\mu\left(\frac{\mu_t}{\mu}\right)\Big|_{2\ layer}, \tag{25}$$

where λ is wall proximity indicator.

Mesh convergence test was conducted to determine the optimum mesh size considering the accuracy and usage of computational resources. Four different mesh sizes of coarse, normal, fine, and very fine were used for this study. The number of cells in each mesh configuration was indicated in Table .1. All the simulations were done for Reynolds number of 15,000. Table 2 shows the values of C_D corresponding to each mesh configurations. From the convergence test, we selected the fine mesh size for further study.

To determine the optimal size of computational domain, a numerical study was conducted. Variations of C_D values were listed at Table 2 according to the change of the upstream length. From Table 2, upstream length of $10w$ is seemed to be a reasonable distance for setting the computational domain size. Also, the downstream length of $20w$ is assessed to be enough, considering the flow

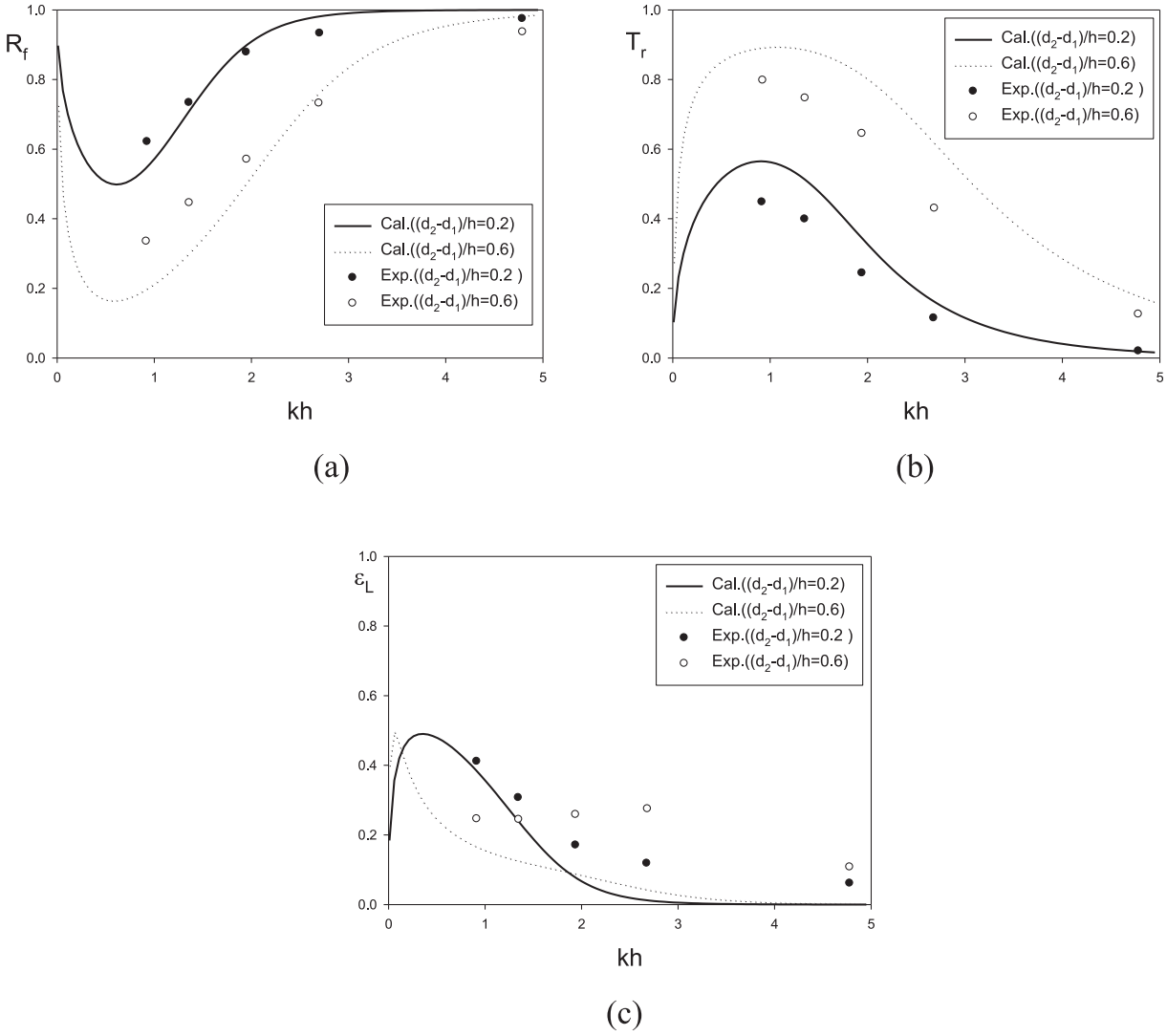

Fig. 6. Comparison of (a) reflection, (b) transmission and (c) energy loss coefficients between the predicted solutions and experimental results as a function of kh and $(d_2 - d_1)/h$ for same height of upper and lower part with $P = 0.5, w = b = 2.5cm, A/\lambda = 0.0125$.

becomes uniform past $8w$ from a barrier.

Fig. 3 shows the velocity pattern around symmetric slats from StarCCM+. The strong water jet through the opening gap is seen due to sudden contraction. It is obvious that due to sudden expansion of cross section, the flow pattern has diverged and turbulent eddies are created in the downstream corners. This zone of recirculating flow with turbulent eddies causes the pressure drop and finally significant energy loss across the slots. Due to the vigorous mixing by the turbulence, the velocity becomes uniform along downstream.

The drag coefficient C_D can be readily obtained by using the $C_D = \Delta P/\frac{1}{2}\rho\overline{U}^2$ derived from Eq. (5) with $C = 0$, where ΔP means the pressure difference between the outer limits of the near field, $\overline{U}$ is the averaged horizontal upstream velocity. The pressure difference ΔP is calculated with two sections which are situated upstream ($8w$) and downstream ($16w$).

As the fitted equation for C_D, we used the thin plate orifice formula (Mei, 1989) multiplied by unknown coefficient α.

$$C_D = \alpha\left(\frac{1}{PC_c} - 1\right)^2 \tag{26}$$

where the empirical form of discharge coefficient C_c for a sharp-edged orifice is

$$C_c = 0.6 + 0.4P^3 \tag{27}$$

Using the numerical results from StarCCM + based on the standard $k - \varepsilon$ model for five different porosities and three different Reynolds numbers, we found out the best fitted value $\alpha = 0.6$ in Eq. (26) through the curve fitting with the StarCCM + numerical results. Fig. 4 shows the fitted curve with $\alpha = 0.6$ together with numerical results marked with symbols. It is found that Reynolds number did not affect energy dissipation. This fitted curve is valid for a slotted barrier with rectangular slats arrayed uniformly, whose porosity range is $0.079 \leq P \leq 0.4265$.

Yoon et al., (2006) and Cho and Koh, (2007) suggested the

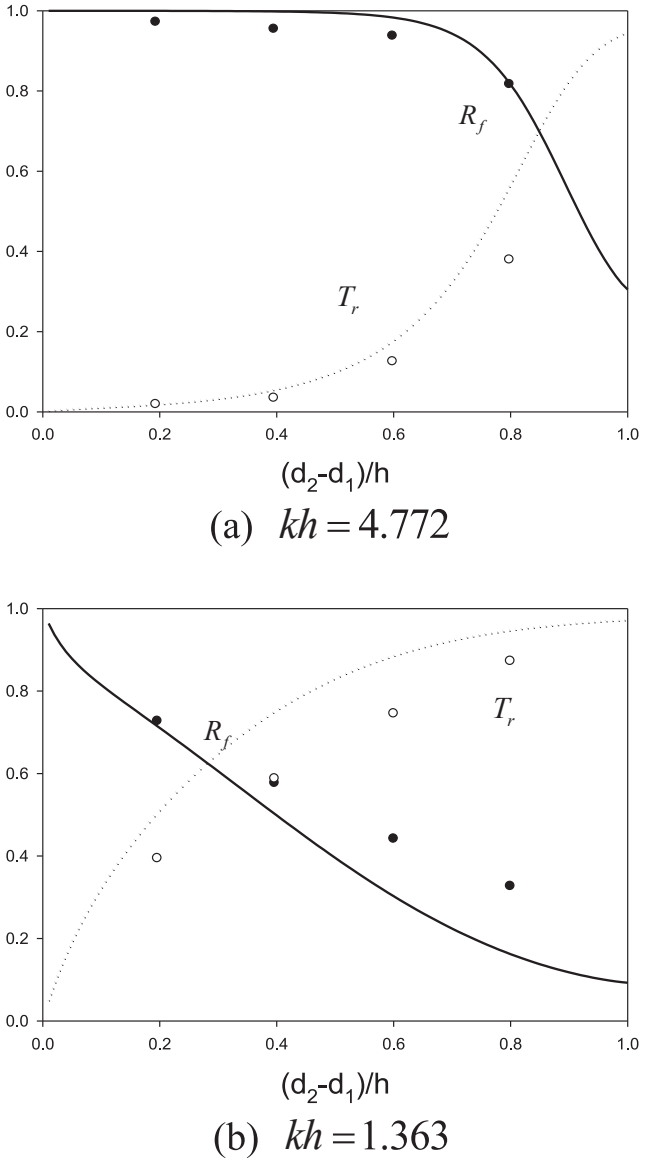

Fig. 7. Comparison of reflection and transmission coefficient between the predicted solutions and experimental results as a function of $(d_2 - d_1)/h$ with $P = 0.5, w = b = 2.5cm, A/\lambda = 0.0125$.

empirical formula for symmetric rectangle and circle slat using FLUENT Spalart-Allmars turbulent model. They showed that rectangular cylinders may help dissipate more wave energy compared with circular cylinders—the enhanced energy loss is due to the flow separation around the sharp edges of the rectangular cylinders.

The effect of varying thickness ratio (b/w) on drag coefficient has also been studied. Four different thickness ratios $(b/w = 0.3, 0.6, 1.0, 2.0)$ were selected for this study. A plot was created between C_D and thickness ratios b/w (Fig. 5). From the figure, it is observed that thickness of a slotted barrier plays less significance in energy dissipation except the lowest porosity value.

3. Numerical results and Discussions

This section contains the comparison of hydrodynamic performance between the theoretical prediction and experimental results for the proposed model. For the comparison, data was taken from the experiments conducted by Ahmed, (2011). The length of the tank is 24 m, and water depth is 0.3 m. Test section is located at a distance of 12.2 m from the wave generator. To measure the reflected and transmitted waves, four wave gauges are installed. The height and thickness of slat are fixed as $w = b = 2.5cm$. The porosity of a slotted breakwater was 0.5.

Fig. 6 shows the comparison of the measured and calculated reflection, transmission, and energy loss coefficients as a function of kh and height of middle part $(d_2 - d_1)/h = 0.2$ and 0.6. The middle part is permeable with a porosity $P = 0.5$, and the impermeable upper and lower part have a same height $(d_1 = (h - d_2))$. It is found that the most important features of the experimental results are well captured by the present theoretical solution, although there is some scatter in the experimental result. The reflection coefficient (R_f) increases with increasing kh at fixed $(d_2 - d_1)/h$ and increases with decreasing $(d_2 - d_1)/h$ for the fixed kh. The transmission coefficient, T_r, follows the opposite trend. In the case of relatively long waves, where $kh \approx 1$, the wave energy is distributed almost uniformly throughout the water depth. As a result, significant part of the wave energy is transmitted through the slotted part of the barrier. As kh increases, the wave energy is concentrated near the still water level. In short wave region, impermeable upper part of the barrier reflects majority of incident wave energy. It causes the increase of R_f and decrease of T_r. As shown in Fig. 6(a and b), ε_L is more significant due to the increase of pressure drop caused by turbulent eddies at low values of kh. For shorter waves, particle velocity is decaying exponentially with distance below the surface. Therefore the drag force, which is proportional to the horizontal fluid velocity, decreases in shorter wave region. Consequently, ε_L is decreasing as kh increases.

Fig. 7(a and b) show the variation of the reflection and transmission coefficients with respect to height of the middle permeable part $(d_2 - d_1)/h$. The impermeable upper and lower parts have a same height. The reflection coefficient R_f decreases with increase of $(d_2 - d_1)/h$, while the transmission coefficient T_r follows the opposite trend as expected. Fig. 7(a) represents the reflection and transmission coefficients for relatively shorter wave. As mentioned in Fig. 6, majority of incident wave energy is reflected from the impermeable upper part of the barrier. Therefore R_f and T_r in Fig. 7(a) shows the even slower variation as increase of $(d_2 - d_1)/h$ than Fig. 7(b).

The importance of the permeable part on the hydrodynamic performance of the vertical slotted breakwater is plotted in Fig. 8(a, b, c). The height of upper part $d_1/h = 0.4$ is fixed while the middle permeable part $(d_2 - d_1)/h$ is varied from 0.2 to 0.4. The increase of height of the middle permeable part increases the energy dissipation in experimental results, whereas decreases the energy dissipation in predicted solutions.

The importance of the impermeable upper part on the hydrodynamic performance of a vertical slotted breakwater is investigated in Fig. 9(a, b, c). From these figures, it is obvious that a change of height in impermeable upper part plays an important effect on hydrodynamic characteristic of the slotted breakwater for all ranges of wavelength. The value of reflection coefficient R_f is about 1 for short waves $(kh > 3.0)$ if the height of upper part is more than $0.4h$ accordingly transmission coefficient is less than 0.1 in this case. For the shorter wave range, a slight change in height of upper part will induce a large variation in the hydrodynamic coefficients. This is because wave energy is more concentrated in the SWL for shorter waves.

Fig. 10 shows the variation of wave force acting on the vertical

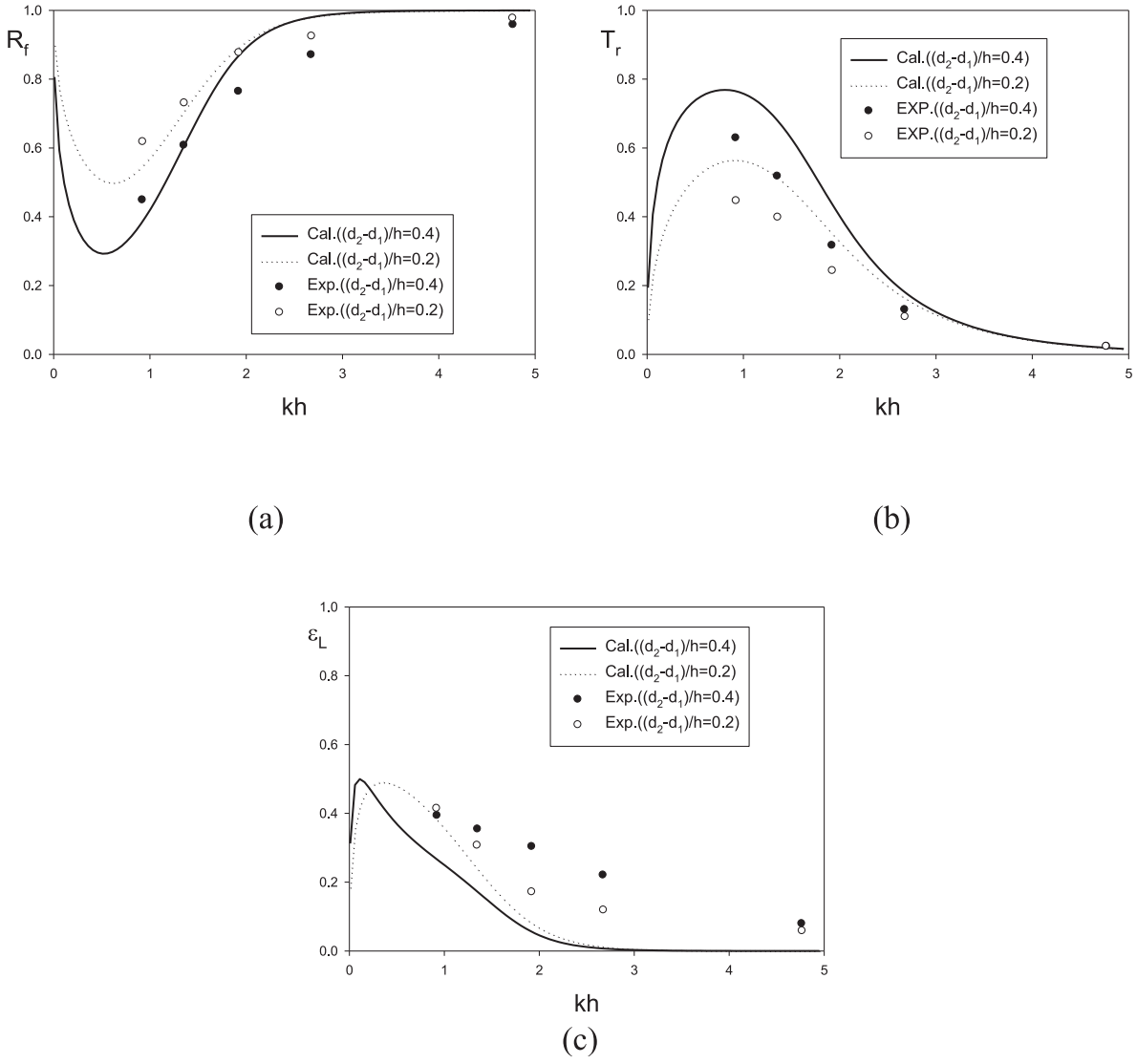

Fig. 8. Comparison of (a) reflection, (b) transmission and (c) energy loss coefficients between the predicted solutions and experimental results as a function of kh and for fixed upper part $d_1/h = 0.4$ with $P = 0.5, w = b = 2.5cm, A/\lambda = 0.0125$.

slotted barrier normalized by the wave force acting on unit width in an impermeable vertical wall extending from seabed to the still water level ($f_0 = 2\rho g A \frac{\tanh kh}{k}$) with three different heights of permeable middle part. It is obvious that the wave force is varying with the heights of middle part only in intermediate and long wave region ($kh < 3.0$). Since energy distribution in short wave region ($kh > 3.0$) is concentrated around upper region of the barrier, there is very less variation in wave forces due to varying middle part heights of the barrier. Fig. 11 shows the variation of normalized wave force ($|f|/f_0$) acting on the vertical slotted breakwater as a function of impermeable upper part's height. In general, all kinds of waves have a significant influence on the wave forces with the upper part's height.

Fig. 12 shows the variation of reflection, transmission, and energy dissipation coefficients of vertical slotted breakwater as a function of kh for different wave steepness. For long and intermediate wave region, there is a meaningful variation in values of reflection and transmission coefficient with different wave steepness. In general it seems that the effects of wave steepness on the reflection and transmission coefficient may not be of practical significance.

Fig. 13 shows the reflection, transmission, and energy dissipation coefficients as a function of porosity, P ranges from 0 to 0.5. The height of the impermeable upper part and permeable middle part of the vertical barrier is fixed. From the figure, it is obvious that the reflection coefficient increases with decreasing barrier porosity, while the transmission coefficient decreases with decreasing barrier porosity. The energy loss coefficient is theoretically zero when either the porosity $P = 0$ or 1, and a maximum energy loss is expected at certain porosity between 0 and 1. From Fig. 13, energy loss coefficient attains a maximum value at a porosity of 0.3.

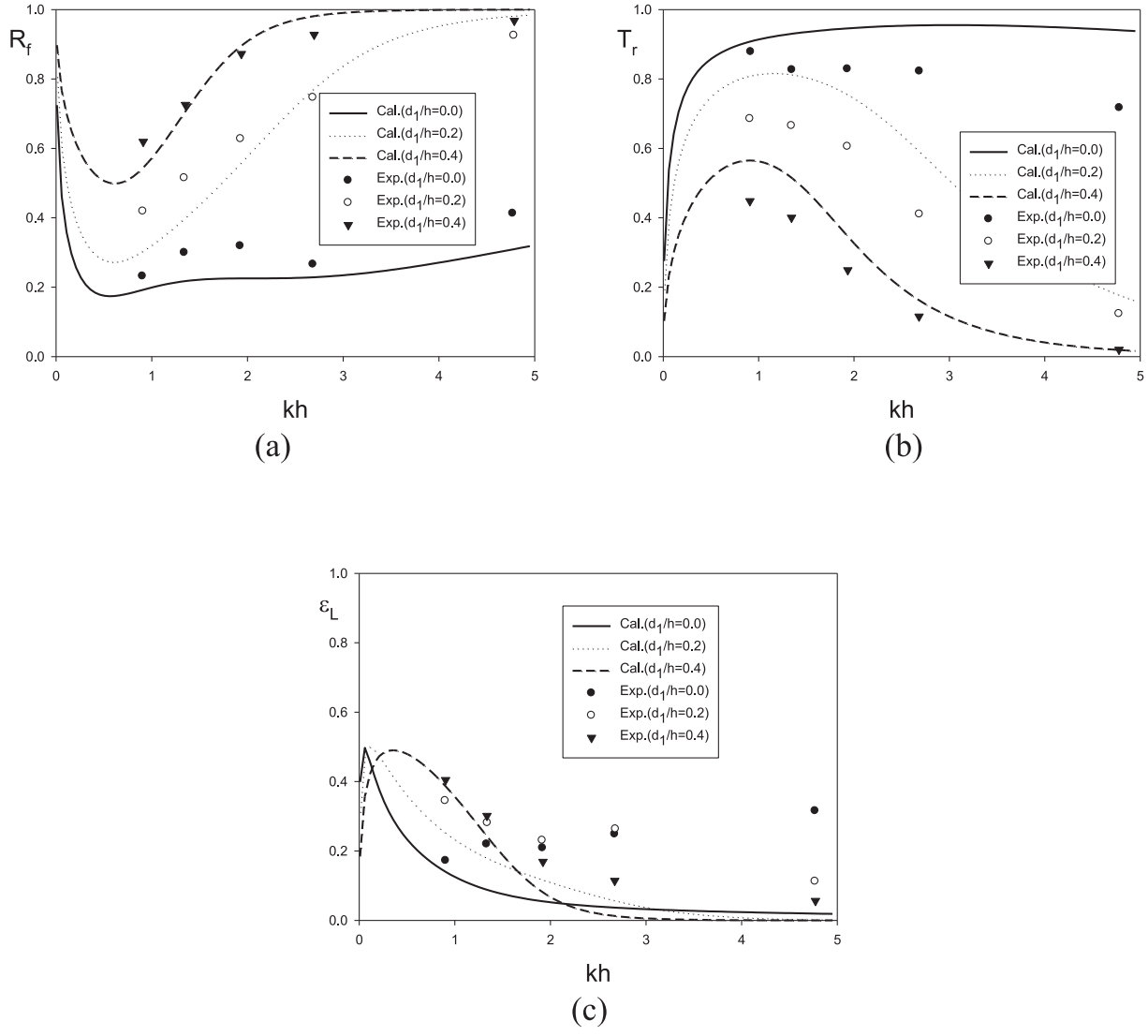

Fig. 9. Comparison of (a) reflection, (b) transmission and (c) energy loss coefficients between the predicted solutions and experimental results as a function of kh and d_1/h for fixed lower part $(h-d_2)/h = 0.4$ with $P = 0.5, w = b = 2.5cm, A/\lambda = 0.0125$.

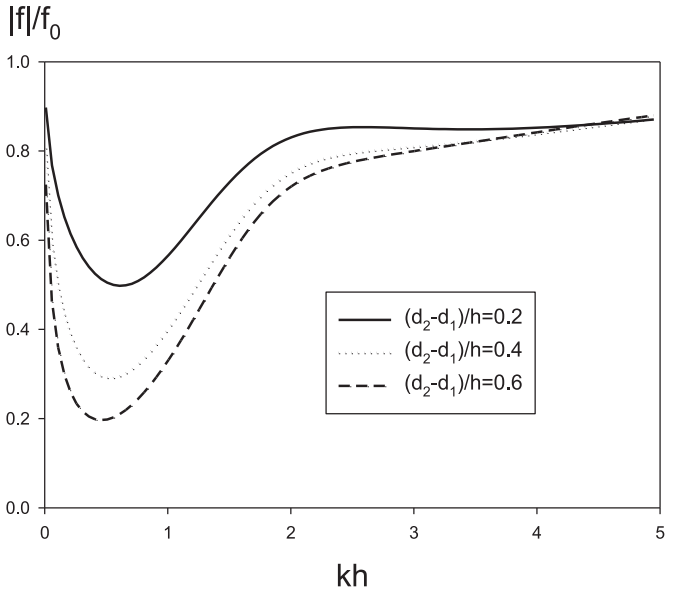

Fig. 10. Wave force acting on vertical slotted breakwater as a function of kh and $(d_2-d_1)/h$ for fixed upper part $d_1/h = 0.4$ with $P = 0.5, w = b = 2.5cm, A/\lambda = 0.0125$.

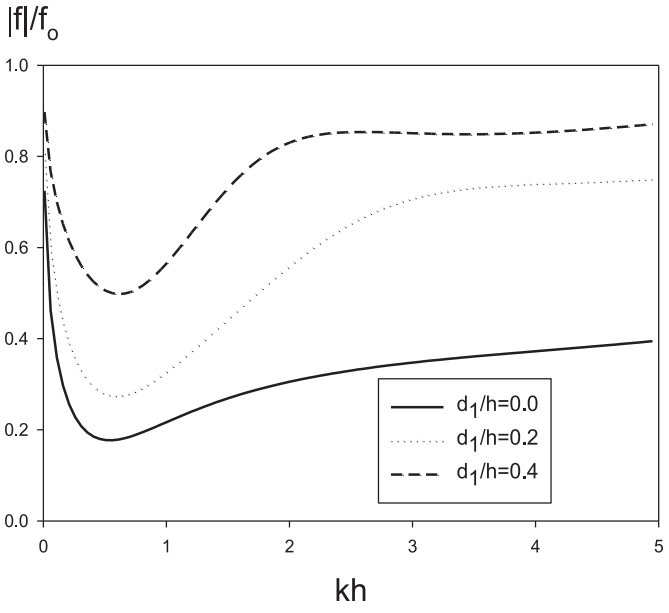

Fig. 11. Wave force acting on vertical slotted breakwater as a function of kh and d_1/h for fixed lower part $(h-d_2)/h = 0.4$ with $P = 0.5, w = b = 2.5cm, A/\lambda = 0.0125$.

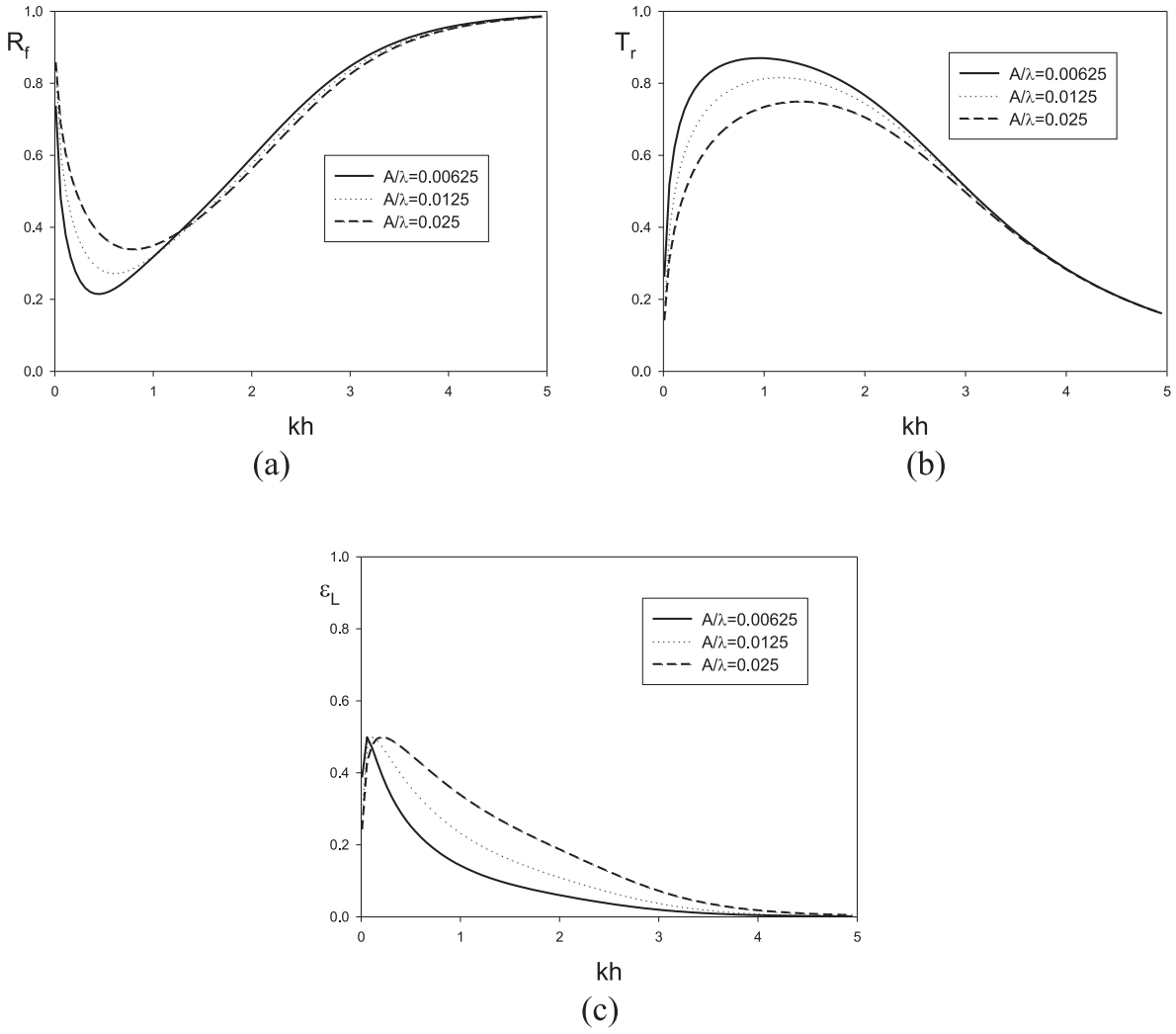

Fig. 12. (a) Reflection, (b) transmission and (c) energy loss coefficients as a function of kh and wave steepness A/λ for $d_1/h = 0.2, (d_2 - d_1)/h = 0.4$ with $P = 0.5, w = b = 2.5cm$.

4. Conclusions

A theoretical model for the estimation of hydrodynamic performance by a slotted vertical breakwater, with impermeable upper and lower parts and permeable middle part, has been presented. The calculation has been conducted with a variety of design parameters of a vertical slotted breakwater under regular waves. The far-field solution incorporated the nonlinear boundary condition applied at the porous barrier. The jump of pressure across the porous barrier is represented by a quadratic drag term with a drag coefficient and a barrier-averaged inertial term with a blockage coefficient. The coefficients were determined empirically in near-field based on the StarCCM+ numerical solution and long-wave approximate solution (Flagg and Newman, 1971). The drag coefficient determined from StarCCM+ was 40% less than Mei's empirical formula. The energy dissipation across the slotted barrier was not sensitive to the Reynolds number and slat's thickness. The nonlinear algebraic equation, in which a quadratic drag law is imposed across the barrier, was solved by the Newton–Raphson iteration technique. Comparisons of the predicted reflection, transmission, and energy loss coefficients with the experimental results of Ahmed, (2011) revealed that the present theoretical model can predict the hydrodynamic performance with reasonable accuracy.

Using the validated predicted tool, the hydrodynamic performance of a vertical slotted breakwater was assessed for various barrier configuration and wave conditions, such as the heights of impermeable and permeable part, porosity, wave steepness, and wavelength. It was seen that an optimal combination of these design parameters existed for given wave characteristics. From the present study, it can be concluded that a properly designed a vertical slotted breakwater can be a candidate for effective port and shore protection method.

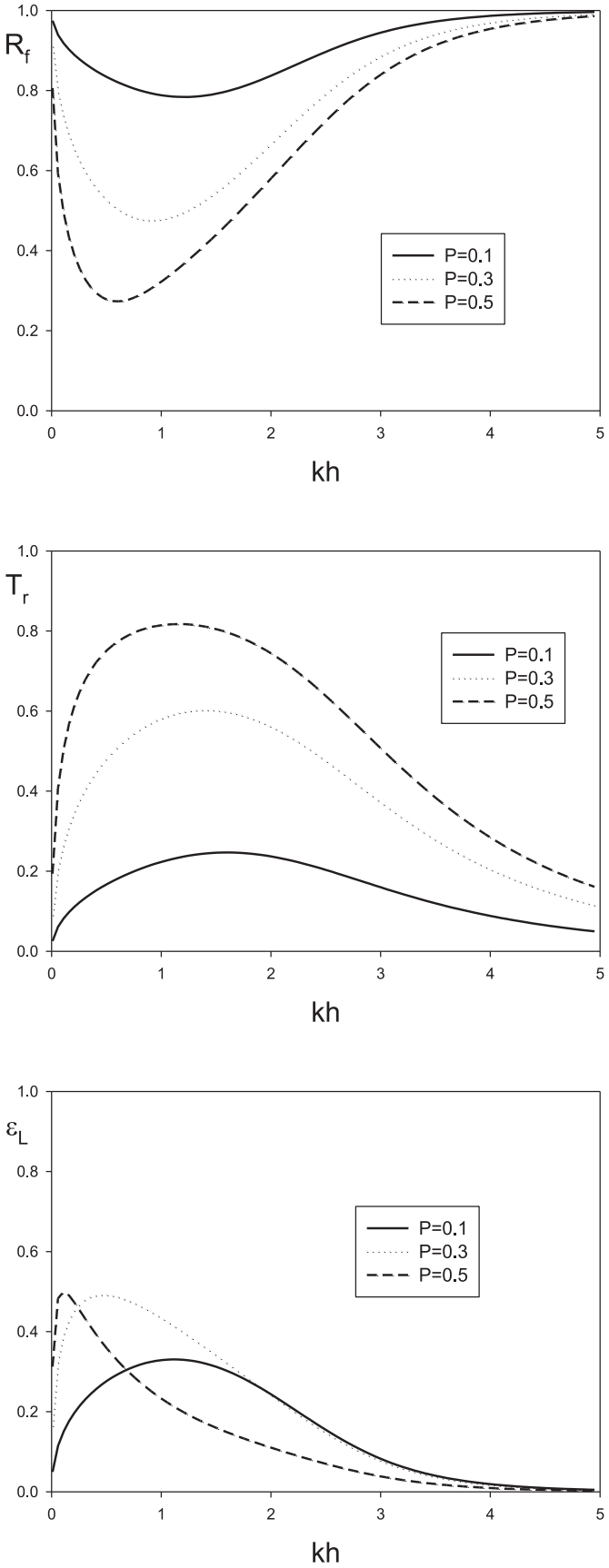

Fig. 13. Reflection, transmission and energy loss coefficients as a function of P and kh for $d_1/h = 0.2, (d_2 - d_1)/h = 0.4$ with $w = b = 2.5cm, A/\lambda = 0.0125$.

Acknowledgments

This research was supported by Basic Science Research Program through the National Research Foundation of Korea (NRF) funded by the Ministry of Education (No.035231).

References

Ahmed, H.G., 2011. Wave Interaction with Vertical Slotted Walls as a Permeable Breakwater. PhD. Thesis, Hydro Sciences (IGAW). Bergische University of Wuppertal, Germany.
Cho, I.H., Kim, M.H., 2008. Wave absorbing system using inclined perforated plates. J. Fluid Mech. 608, 1–20.
Cho, I.H., Koh, H.J., 2007. Reflection and transmission coefficients by a circular pile breakwater. Journal of Korean Society of Coastal and Ocean Engineers 19 (1), 38–44 (in Korean).
Crowley, S., Porter, R., 2012. The effect of slatted screens on waves. J. Eng. Math. 76, 53–76.
Flagg, C.N., Newman, J.N., 1971. Sway added-mass coefficients for rectangular profiles in shallow water. J. Ship Res. 15, 257–265.
Grüne, J., Kohlhase, S., 1974. Wave transmission through vertical slotted walls. In: Proc., 14th Coastal Engineering Conference, ASCE, vol. 3, pp. 1906–1923.
Hayashi, T., Hattori, M., Kano, T., Shirai, M., 1966. Hydraulic research on the closely spaced pile breakwater. Coastal Engineering in Japan 9 (1), 107–117.
Huang, Z., 2007. Reflection and transmission of regular waves at a surface-pitching slotted barrier. Appl. Math. Mech. 28 (9), 1153–1162.
Isaacson, M., Premasiri, S., Yang, G., 1998. Wave interactions with vertical slotted barrier. J. Waterw. Port, Coast. Ocean Eng. 124 (3), 118–126.
Kakuno, S., Liu, P.L.F., 1993. Scattering of water waves by vertical cylinders. J. Waterw. Port, Coast. Ocean Eng. 119 (3), 302–322.
Kriebel, D.L., 1993. Vertical wave barriers: wave transmission and wave forces. In: Coastal Engineering, pp. 1313–1326.
Mei, C.C., 1989. The applied dynamics of ocean surface waves. In: World Scientific, Singapore. World Scientific, Singapore.
Mei, C.C., Liu, P.L.F., Ippen, A.T., 1974. Quadratic loss and scattering of long waves. J. Waterw. Harb. Div. 100 (3), 217–239.
Molin, B., Remy, F., 2013. Experimental and numerical study of the sloshing motion in a rectangular tank with a perforated screen. J. Fluids Struct. 43, 463–480.
Sollit, C.K., Cross, R.H., 1972. Wave transmission through permeable breakwaters. In: Proc. 13th Coastal Engineering Conference. ASCE, pp. 1827–1846.
Somervell, L.T., Thampi, S.G., Shashikala, A.P., 2017. Hydrodynamic characteristics of vertical cellular breakwater. J. Waterw. Port, Coast. Ocean Eng. 143 (5).
Suh, K.D., Park, W.S., 1995. Wave reflection from perforated-wall caisson breakwaters. Coast. Eng. 26 (3–4), 177–196.
Suh, K.D., Shin, S., Cox, D.T., 2006. Hydrodynamic characteristics of pile-supported vertical wall breakwaters. J. Waterw. Port, Coast. Ocean Eng. 132 (2), 83–96.
Suh, K.D., Kim, Y.W., Ji, C.H., 2011. An empirical formula for friction coefficient of a perforated wall with vertical slits. Coast. Eng. 58 (1), 85–93.
Yoon, S.B., Lee, J.I., Nam, D.H., Kim, S.H., 2006. Energy loss coefficient of waves considering thickness of perforated wall. J. Korean Society of Coastal and Ocean Engineers 18 (4), 321–328 (in Korean).